This is the preprint version of the following article:
Nicholas C. Orndorff, and John T. Hwang. Air-taxi trajectory optimization with aerodynamic and motor models. Journal of Aircraft, 2023.
Preprint pdf: https://github.com/LSDOlab/lsdo_bib/blob/main/pdf/orndorff2023trajopt.pdf
Bibtex: https://github.com/LSDOlab/lsdo_bib/blob/main/bib/orndorff2023trajopt.bib

Air-taxi trajectory optimization with aerodynamic and motor models

Nicholas C. Orndorff* and John T. Hwang†

University of California San Diego, La Jolla, CA, 92093

Abstract

Many air-taxi concepts are capable of vertical takeoff and landing, enabling them to fly to and from urban locations. An important capability for these air taxis is the transition between hover and forward flight. We propose a robust methodology for computing optimal takeoff and transition trajectories using surrogate models trained on data from physics-based models. The use of surrogate models reduces the computational complexity and improves the robustness of the trajectory optimization algorithm. We demonstrate the versatility and robustness of the proposed methodology by applying it to 12 trajectory optimization problems that involve air-taxi takeoff and outbound transition. These trajectories are representative of real air-taxi operations, with a variety of constraints derived, in part, from proposed mission requirements.

Nomenclature

v	=	velocity (m/s)	L, D	=	lift, drag (N)
γ	=	flight path angle (rad)	C_L, C_D	=	lift/drag coefficients
h	=	altitude (m)	C_T, C_P	=	thrust/power coefficients
x	=	horizontal position (m)	T, P, Q	=	thrust (N) power (W) and torque (N-m)
α	=	angle of attack (rad)	ρ	=	density (kg/m^3)
θ	=	pitch angle (rad)	d_C, d_L	=	cruise and lift rotor diameter (m)
m	=	mass (kg)	n	=	rotor speed (revolutions/s)
g	=	acceleration due to gravity (m/s^2)	η	=	efficiency (%)
T_C, T_L	=	cruise thrust and lift thrust (N)			

A version of this paper was originally presented at the *AIAA SciTech 2023 FORUM* held in National Harbor, MD on January 23-27, 2023. Paper number: AIAA 2023-0324. https://doi.org/10.2514/6.2023-0324

*PhD Student, Department of Mechanical and Aerospace Engineering
†Assistant Professor, Department of Mechanical and Aerospace Engineering

1 Introduction

Electric air-taxi concepts are rapidly being developed to meet the vision for large-scale urban air mobility (UAM). To fulfill this vision, aircraft designers must carefully model and analyze a wide variety of systems and design conditions that span a number of engineering disciplines. As such, air-taxi design is a problem that is well-suited to benefit from large-scale multidisciplinary design optimization (MDO). Within a large-scale MDO framework, an entire aircraft concept can be analyzed and optimized in the presence of many, perhaps hundreds of variables and constraints.

Large-scale MDO has been applied to the design of air-taxis [1, 2] and the system-level design of electric aircraft [3]. These examples of aircraft design optimization consider multiple steady mission segments, that provide a reasonable approximation of the complete mission profile. However, many proposed air-taxi missions include significant dynamic mission segments [4, 5]. These segments primarily occur at the start and end of each UAM mission, when the air taxi must transition between hover and cruising flight [6, 7]. This transition is characterized by highly nonlinear flight dynamics and complex interactions between the aircraft and the environment. Because of this complexity, optimal trajectories are not necessarily intuitive. One method of finding these trajectories is to apply a trajectory optimization algorithm within an MDO framework [6, 8, 9].

Trajectory optimization problems are typically solved with one of three techniques: dynamic programming, indirect methods, and direct methods [10, 11]. Dynamic programming yields a globally optimal solution but relies upon a discretized state space which it often must explore in its entirety [12]. Because of this, dynamic programming is best suited to small state spaces and discrete dynamics. More complex problems are often solved by indirect or direct methods [13]. Indirect methods rely upon the analytical derivation of the necessary conditions for optimality [10]. These conditions depend upon the system model and constraints, and must be re-derived whenever the problem is modified. Direct methods start by discretizing the system and then applying optimization. Generally, the discretized system is transcribed as a nonlinear programming (NLP) problem that can be solved using established gradient-based optimization methods [14, 15]. With direct transcription, there is no need to analytically derive the problem-specific necessary conditions for optimality [8]. Because of this, direct transcription is well-suited to complex problems with constraints and models that rapidly evolve (e.g., the aircraft design process).

The conversion from an optimal control problem to a nonlinear program requires both discretization and simulation. Generally, continuous-time systems are discretized by introducing collocation points that represent finite points in time where controls and constraints can be defined [10]. The state values at the collocation points are defined through simulation. Simulating trajectories by explicitly propagating states across the collocation points is known as "shooting" and typically makes use of standard ODE solution methods [8]. Hwang and Munster [16] applied the general linear methods (GLM) approach in the development of an ODE solver within an MDO framework. The GLM method simplifies the implementation of collocation within an NLP problem by allowing rapid implementation of multiple integration methods. In order to combine the GLM method with gradient-based optimization, the derivatives of the resulting ODE representation must be provided. These can be computed using the modular analysis and unified derivatives approach [17, 18].

Direct trajectory optimization has been successfully applied to a wide variety of aerospace applications. For example, Blackmore et al. [19] used direct methods to develop a Mars landing guidance algorithm that minimizes the landing target error given specific fuel constraints. By formulating the dynamics and constraints to be convex, they guarantee finite-time convergence to

an optimal solution. However, the physical phenomena we wish to model are complex, and it is difficult to create a convex problem. In this case, convergence of the NLP is not guaranteed and the complexity of the models used plays a large role in determining the feasibility of the optimization problem. Despite this, there are many examples of successful trajectory optimization problems with complex and nonlinear models. In one relevant example, Chauhan and Martins [6] used nonlinear physics-based models to find optimal takeoff and transition trajectories for the Airbus Vahana tilt-wing air taxi with a variety of wing loading and stall constraints. Other examples include the optimization of supersonic minimum-time-climb trajectories [20, 21], rocket ascent and evasive maneuvers [22], and electric aircraft trajectories subject to thermal constraints [23].

In certain cases, physics-based models are too computationally expensive to include within a trajectory optimization problem due to limitations on computer power and time. In other cases, these models may contain numerical singularities (e.g., equations might become undefined when certain variables are zero). These possibilities hurt the robustness of the optimization algorithm. Anderson et al. [7] evaluated the effect of model fidelity for trajectory optimization of a small bi-wing tailsitter aircraft. They specifically evaluated rotor-wing interactions, and found that higher-fidelity models were significantly more conservative when predicting rotor power and wing stall. This example highlights the importance of using higher-fidelity models in trajectory optimization. One method of reducing model complexity while maintaining model fidelity is to use surrogate models [24–27]. This approach generates data offline using the original physics-based model. A function can then be fit to the data and used as a surrogate model within the trajectory optimization problem. Because these surrogate models are often simple continuous functions, they are robust and fast to evaluate. The popularity of surrogate modeling within MDO problems has led to the creation of several surrogate modeling toolboxes that include a variety of functions and allow easy access to derivatives [28, 29].

In this paper we use direct transcription and fast surrogate models to find optimal takeoff and transition trajectories for NASA's Lift-plus-Cruise air-taxi concept [4, 30] (Figure 1). We use four physics-based models: flight dynamics, lifting-surface aerodynamics, rotor aerodynamics, and motors. With the exception of the flight dynamics model, the other three models are used to train new surrogate models that are evaluated within the optimization algorithm. Every model is written in the Computational System Design Language (CSDL) [31], which leverages a computational graph to automatically derive models for computing all the derivatives required for optimization.

We begin by describing our methodology in Section 2. This includes a description of the individual physics-based models, their corresponding surrogates, and the complete optimization problem formulation. Next, we present our results in Section 3. This section demonstrates the robustness of our approach by using the same models and problem formulation to compute 12 air taxi takeoff and transition trajectories that satisfy minimum-energy and minimum-time objectives. Our goal with these results is to show that the fast surrogate modeling approach is not purely academic, and can be directly applied to complex real-world trajectories. To date, little research exists that shows optimal trajectories for large air taxis. Therefore these results also begin to answer the question: what do optimal takeoff and transition trajectories look like? We conclude by summarizing our results and research contributions in Section 4.

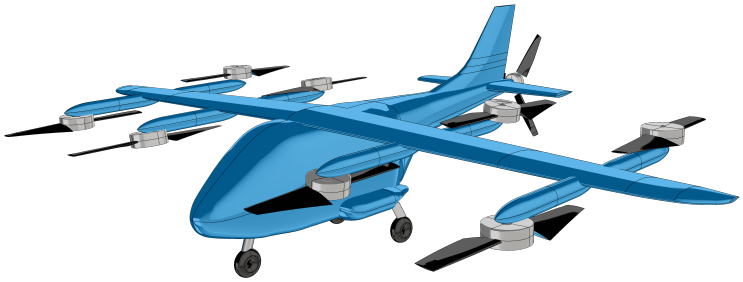

Figure 1: NASA's Lift-plus-Cruise air-taxi concept [4].

2 Methodology

In this section we present four physics-based models for flight dynamics, wing aerodynamics, rotor aerodynamics, and motors. When combined, these models represent all the key disciplines relevant in air-taxi takeoff and transition trajectory design. Because air-taxi trajectories traverse a wide range of flight regimes, we paid close attention to the following three areas when developing these models:

1. *Robustness*: the models must accept a wide range of inputs (e.g., angles of attack within $\pm 90°$)
2. *Validity*: the models must be accurate across many operating conditions (e.g., Mach numbers between 0 and 0.3)
3. *Efficiency*: the model evaluations must be inexpensive (surrogate models reduce the computation time).

Surrogate models are used to improve the computational complexity of model evaluations. Often, the physics-based models described in this section are slow (due to the inherent complexity required to model the phenomena in question) or they contain numerical singularities (e.g., when inputs go to zero). However, by training surrogate models based on data generated offline, we can significantly improve the robustness and speed of the optimization algorithm. Figure 2 shows an evaluation-time comparison between the original physics-based models and their corresponding surrogate models.

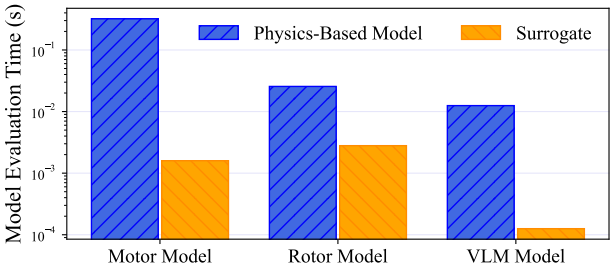

Figure 2: Model evaluation time comparisons between the original physics-based models and their surrogate-based counterparts (averaged over 40 samples).

2.1 Flight Dynamics

Aircraft trajectories are simulated with a three-degree-of-freedom flight dynamics model. The following four equations allow for the explicit propagation of the aircraft velocity (v_x and v_z), the horizontal position (x), and the altitude (h) with respect to time:

$$m\dot{v}_x = T_c \cos\theta - T_l \sin\theta - D\cos\gamma - L\sin\gamma \tag{1}$$

$$m\dot{v}_z = T_c \sin\theta + T_l \cos\theta - D\sin\gamma + L\cos\gamma - mg \tag{2}$$

$$\dot{h} = v_z \tag{3}$$

$$\dot{x} = v_x. \tag{4}$$

Figure 3 depicts these four aircraft states and their corresponding coordinate systems. The inputs to these equations are the lift and cruise rotor thrust (T_c, T_l), the pitch angle (θ), the flight-path angle ($\gamma = \tan^{-1}(v_z/v_x)$), lift ($L$), and drag ($D$). In previous work [32], we found that (a) the difference in thrust between the front and rear sets of lifting rotors that is required to generate a large pitching moment is negligible, and (b) the difference in inflow velocities due to aircraft rotation is also negligible. Consequently, we reduce the computational complexity of the model by analyzing a single lift rotor and multiplying the thrust and power by k lift rotors to get the total lift rotor thrust and the total lift rotor power (e.g., $T_L = kT$). This approach makes the assumption that the aircraft is capable of instantaneously tracking any commanded pitch angle.

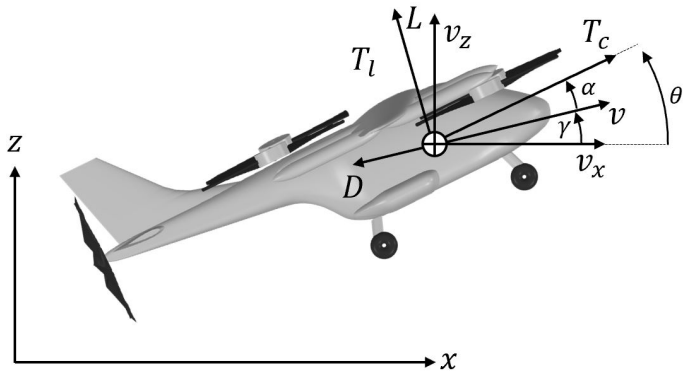

Figure 3: Coordinate system for the 3-DOF flight dynamics model.

2.2 Rotors

Blade-element-momentum (BEM) rotor models have been successfully included in air-taxi trajectory optimization problems [32][9]. However, these BEM implementations only guarantee accuracy for axial inflow velocities. Air-taxi transition trajectories inherently contain large segments of edgewise flight that result in large tangential inflow velocities. We account for this by implementing the dynamic inflow rotor model developed by Pitt and Peters [33, 34]. The Pitt-Peters

model accounts for edgewise flight with three inflow states that represent the uniform, side-to-side, and fore-to-aft flow variations respectively. These inflow parameters are combined with standard blade element theory to compute thrust and moment coefficients (C_T, C_{M_y}, and C_{M_x}). The thrust and power coefficients (C_T, and C_P) in the rotor axes are found via a simple transformation of the thrust and moment coefficients. To simplify the implementation of this rotor model, we use surrogate models for C_T, and C_P. The surrogate models are created with regularized minimal-energy tensor-product splines (RMTS) [35] using the surrogate modeling toolbox (SMT) developed by Bouhlel et al. [28]. Figure 4 shows a subset of the surrogate models created for the cruise rotor. Rotor thrust, torque, and power (T, Q, and P) are calculated using these surrogate models and the rotor diameter (d) (see d_C and d_L in Table 1), rotations per second (n), and the atmospheric density (ρ) (computed from a standard atmosphere model):

$$T = \rho n^2 d^4 C_T \tag{5}$$

$$P = \rho n^3 d^5 C_P \tag{6}$$

$$Q = \rho n^2 d^5 C_Q. \tag{7}$$

The torque coefficient C_Q is found as a function of the power coefficient: $C_Q = C_P/2\pi$. To compute the total aircraft power we sum the individual rotor powers (with k lifting rotors): $P = P_{\text{Cruise}} + kP_{\text{Lift}}$. The total energy E consumed by the aircraft is expressed as an additional ordinary differential equation: $\dot{E} = P$. The total energy used by the aircraft for a given trajectory is the final entry in the resulting discrete-time energy vector.

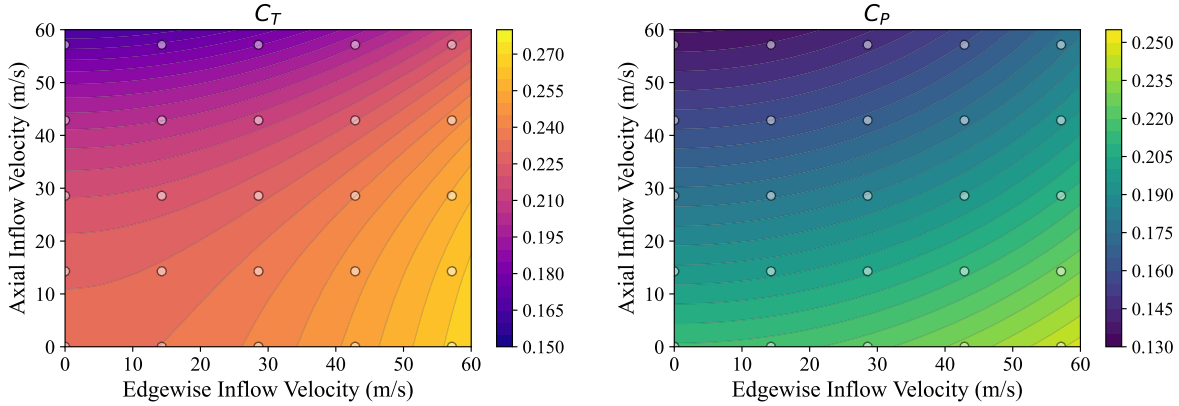

Figure 4: Cruise rotor surrogate models for thrust and power coefficients (C_T and C_P) as a function of axial and edgewise free-stream velocity. Dots represent the training points for the model.

2.3 Aerodynamics

Aircraft aerodynamics are analyzed using standard lift and drag equations: $L = \frac{1}{2}\rho v^2 s C_L$ and $D = \frac{1}{2}\rho v^2 s C_D$, where s is the wing area (see Table 1 for aircraft specifications), and ρ is the atmospheric density computed, as above, from a standard atmospheric model. The lift and drag coefficients (C_L and C_D) are found in a surrogate model that spans a wide range of angle of attack values ($\pm 90°$) (Figure 5). This is necessary since vertical flight near hover can result in angles of

attack that extend to ±90°. These surrogate models are constructed with radial basis functions (RBF) [36] using the SMT toolbox [28] based in part on vortex lattice method analyses performed in OpenVSP [37] and extrapolated to high α using computational fluid dynamics data from Petrilli et al. [38] and experimental data presented by Sheldahl and Klimas [39].

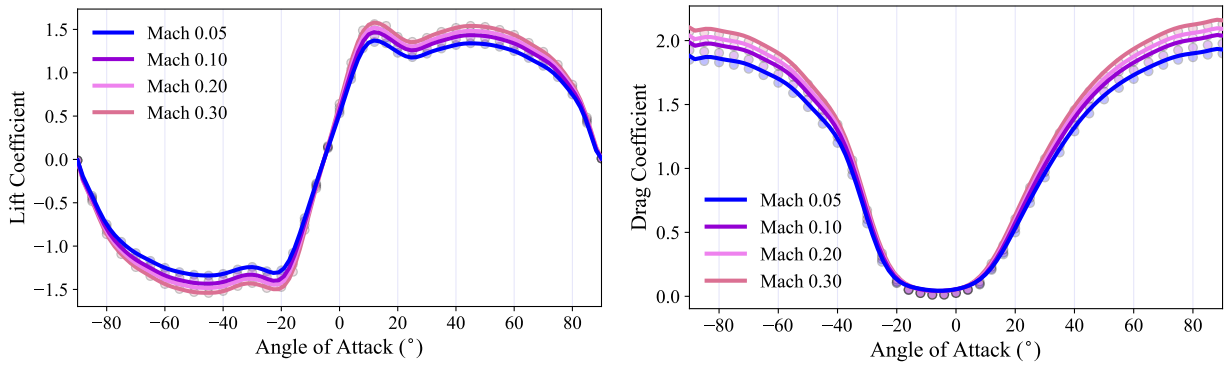

Figure 5: The aerodynamic surrogate model for lift and drag coefficients.

Table 1: Lift-plus-Cruise aircraft specifications

Parameter (m)	Value
Mass (m)	3000 kg
Wing area (s)	19.6 m^2
Cruise / lift rotor diameters (d_C, d_L)	2.6 m / 2.4 m
Number of lift rotors	8
Cruise / lift rotor blades	3 / 2

2.4 Motors

We account for the effects of motor efficiency by including a motor efficiency map. We begin by calculating the basic motor geometry using a sizing model based on empirical relationships [40]. These relationships represent the internal motor geometry as a function of two high-level parameters: stator diameter and motor length. Next, the outputs of the sizing model are inputs to a second model, which calculates the motor efficiency map as a function of load torque and motor speed by solving the following residual: $r = \eta\tau_{EM} - \tau_{load} = 0$.

The motor analysis model is formulated as an implicit function in order to relate the unknown electromagnetic torque τ_{EM} and efficiency η to the load torque τ_{load}. The motor power and current are calculated with two discrete control modes: flux weakening [41] and maximum torque per ampere [42]. These modes govern motor operation at the voltage limit ($V_{lim} = 400$ V) and below the voltage limit respectively. We note that air-taxi motors are not expected to operate in the flux-weakening regime, and we include this mode entirely for model robustness. These models are used to generate motor efficiency maps (Figure 6). We train an RBF surrogate model to approximate this map, with which we calculate the total power as a function of the ideal rotor power $P = P_r/\eta$.

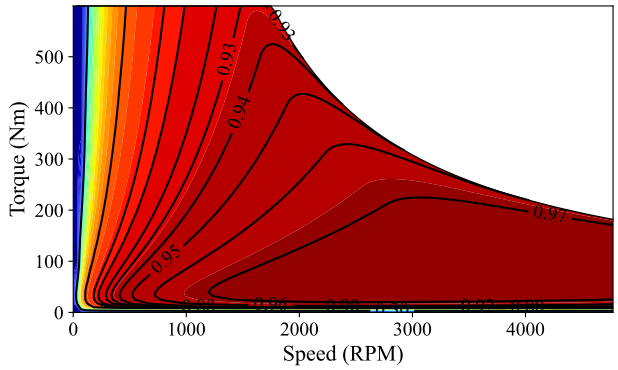

Figure 6: The motor efficiency map surrogate model: $\eta = f(\tau, n)$.

2.5 Trajectory Optimization

We begin by describing the trajectory optimization problem with an optimal control representation in continuous time. The system dynamics are described in a general form: $\dot{x} = f(t, x(t), u(t))$, and we aim to find control profiles $u(t)$ that minimize a certain objective function $J = \phi(t, x(t), u(t))$. The resulting state trajectories $x(t)$ must satisfy certain path and terminal constraints (c_p and c_t). The complete optimal control representation is summarized as:

$$\begin{aligned} \underset{u(t)}{\text{minimize}} \quad & J = \phi(t, x(t), u(t)) \\ \text{subject to} \quad & \dot{x} = f(t, x(t), u(t)) \\ & c_p(t, x(t), u(t)) \leq 0 \\ & c_t(t_f, x(t_f), u(t_f)) = 0. \end{aligned} \tag{8}$$

We consider two objectives: energy and time. Energy is calculated as the integral of total motor power $E = \int P(t, x(t), u(t))dt$, and time is represented by the integrator time step Δt where $t_f = N\Delta t$ for N time steps. Using direct transcription, we reformulate the continuous-time optimal control problem in a discrete-time form for the minimum energy objective:

$$\begin{aligned} \underset{\mathbf{u}, \Delta t}{\text{minimize}} \quad & E = \textstyle\sum_{t=0}^{t_f} P(x_t, u_t), \forall \mathbf{t}, \mathbf{x}, \mathbf{u} \in R^{N+1} && \text{(objective function)} \\ \text{subject to} \quad & \dot{\mathbf{x}} = f(\mathbf{t}, \mathbf{x}(t), \mathbf{u}(t)) && \text{(system dynamics)} \\ & c_p(\mathbf{x}, \mathbf{u}) \leq 0 && \text{(path constraints)} \\ & c_t(\mathbf{x}, \mathbf{u}) = 0 && \text{(terminal constraints)} \\ \text{with} \quad & \mathbf{t} = [t_i, t_i + \Delta t, t_i + 2\Delta t, \ldots, t_i + N\Delta t] && \text{(discrete time vector).} \end{aligned} \tag{9}$$

For the minimum time objective, we minimize the time step Δt instead of the energy E in (9). We consider three dynamic variables (vectorized across time) as the inputs u: pitch angle, cruise rotor speed, and lift rotor speed. We include a single scalar input: the integrator time step Δt. Since the number of time steps is a fixed quantity (N), Δt is effectively a method of adjusting the total time t_f.

The aircraft trajectories are simulated with a fourth-order Runge-Kutta integration scheme using initial conditions that are derived from a steady hovering condition at an initial altitude h_i ($v_0 = 0.1$ m/s, $\gamma_0 = 0°$, $x_0 = 0$ m, and $h_0 = h_i$), (v_0 is slightly positive so that the flight-path

angle remains defined). The maneuver is considered complete when several terminal constraints are satisfied (h_f, v_f, and γ_f). Path constraints are comprised of a variety of practical aircraft and trajectory limitations. For example, rotor power is constrained by the maximum available power, and the minimum altitude is constrained by ground collisions and no-fly zones. There are two constraints motivated by passenger comfort. First, the pitch angle is constrained to be less than 20° (the typical airliner maximum pitch angle during takeoff is approximately 20° [43]). Second, we constrain the maximum acceleration (in any direction) to be no greater than 0.5g, a value determined by Gebhard [44] to be the maximum acceleration that passengers can endure without discomfort. All path constraints are implemented using maximum and minimum operators across time-instances in state vectors (approximated with Kreisselmeier–Steinhauser (KS) functions [45]) in order to reduce the total number of constraints and increase the optimization speed. The complete optimization problem is summarized in Table 2.

In Section 3.3, we include a single obstacle constraint that enforces a no-fly zone. The no-fly zone altitude is given by a function of the horizontal position ($h_{NFZ} = h(x)$). This function is then used to construct a residual $r = (h - h_{NFZ})$ which we constrain to always be greater than or equal zero. This constraint is not mathematically rigorous because it is only enforceable at the collocation points of the NLP, and the trajectory between these points can violate the no-fly zone. However, in practice the collocation points are close-enough together that this is not a significant limitation. This constraint formulation allows us to rapidly evaluate different obstacle geometries without changing the optimization problem. The obstacle function h_{NFZ} is constructed using radial basis functions in SMT [28]. This provides the freedom to generate obstacles of nearly any smooth shape, which in this paper consists of a sinusoidal ramp to a constant altitude (Figure 11).

Table 2: Optimization problem formulation

		Variable/Description	Quantity (N timesteps)
Objective	Energy or time	$J = E$, Δt	
Design variables	Lift rotor speed	n_L	N
	Cruise rotor speed	n_C	N
	Pitch angle	θ	N
	Timestep	Δt	1
			Total design variables: $(3N + 1)$
Constraints	Maximum lift power	$\max P_L \leq 103,652$ W	1
	Maximum cruise power	$\max P_C \leq 468,300$ W	1
	Final altitude	$h_f = 300$ m	1
	Minimum altitude	$\min h \geq 0$ m	1
	Maximum acceleration	$\max \lvert\dot{v}/g\rvert \leq 0.5$ g	1
	Maximum pitch angle	$\max \lvert\theta\rvert \leq 20°$	1
	Final velocity	$v_f = 58$ m/s	1
	Final flight path angle	$\gamma_f = 0°$	1
			Total constraints: 8
Other constraints	No-fly zone	$\min (h - h_{NFZ}) \geq 0$	1

We solve the discretized optimization problem with gradient-based optimization leveraging the automatic adjoint-based derivative computation enabled by our use of CSDL. The computational expense of adjoint derivative computation scales well with the number of design variables, and is well suited to large-scale MDO. The optimizer is SNOPT-7.7 [46] (a sparse nonlinear optimizer), which in most cases converges to an optimal solution within 30 minutes using a desktop computer

with an Intel i7-13700K processor and 32GB of memory. The system is discretized with $N = 40$ time steps, a number that is empirically determined to provide sufficient resolution without unnecessary computation time. This results in a nominal optimization problem with 121 design variables and eight constraints.

Certain variables such as power are large (approx. 10^6) while others are small such as angle of attack (approx. 10^{-2}). This leads to a poorly conditioned problem that struggles to converge. We address this by scaling the design variables, constraints, and the objective before optimization. For variables that are roughly constant, we accomplish this by multiplying the variable by the inverse of the expected value. Once properly scaled, we converge all our results to an optimality and feasibility tolerance of 10^{-8}.

3 Results

Using the problem formulation described above, we now present optimal transition trajectories for the minimum-energy and minimum-time objectives. We characterize these trajectories by plotting the time histories of the system states (x, h). To gain further insight, we also plot functions of the states (e.g., power vs. time).

To facilitate comparisons between trajectories, we use a transition efficiency parameter η as defined by Chauhan and Martins [6]. This parameter computes the ratio of the increase in mechanical energy (kinetic plus potential energy) to the total energy consumed by the aircraft:

$$\eta = (0.5m\Delta v^2 + mg\Delta h)/E. \tag{10}$$

This equation is equivalent to the ratio of the specific energies (energy per unit mass), and enables comparisons between different trajectories and different aircraft configurations.

3.1 Optimal Transition and Takeoff Trajectories

The first two trajectories that we explore are minimum-energy and minimum-time transition. For these results, the aircraft begins at hover and must transition to cruise at the same altitude. The key feature of these trajectories is that the altitude is not fixed during transition; that is, the aircraft is free to climb/dive to whatever extent is necessary to minimize the objective function. The minimum energy and minimum time transition trajectories are shown in Figure 7. In every figure that follows, the aircraft markers are equally spaced with respect to time and the marker rotation indicates the instantaneous pitch angle.

Each trajectory in Figure 7 exhibits distinctive behaviors. First we examine the minimum-energy transition trajectory. This trajectory is characterized by an initial dive, followed by a climb back to the initial altitude. By following this path, the aircraft trades potential energy for kinetic energy (by diving) and is able to switch to full wing-based lift as early as possible. This minimizes any reliance on the lifting rotors, which are less efficient at generating lift than the wing. Second, we examine the minimum-time transition trajectory. This trajectory shows a rapid initial acceleration, similar to how a conventional helicopter accelerates in a nose-down configuration (with a negative pitch angle). However, a helicopter accelerates in this way due to the balance of forces and moments. For the Lift-plus-Cruise aircraft, this nose-down acceleration is the fastest way of reaching the cruise velocity while maintaining enough lift to avoid large excursions from the shortest path (a straight line).

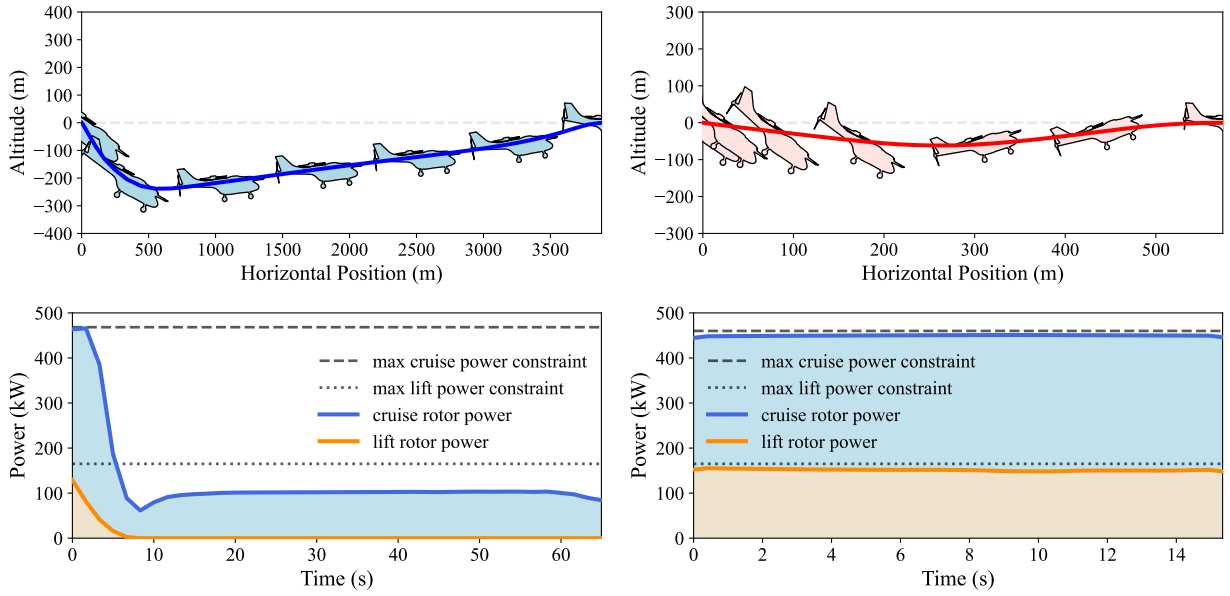

Figure 7: Top left: the minimum-energy transition trajectory. Top right: the minimum-time transition trajectory. Bottom left: the power profiles for the minimum-energy transition. Bottom right: the power profiles for the minimum-time transition.

Further comparisons between these two transition trajectories are evident by plotting the time-histories of the cruise and lift rotor power (Figure 7). Notably, the minimum-time transition trajectory uses near-maximum power for all rotors for the full duration of the transition. The power never quite reaches the maximum power constraint likely because the KS function (used to aggregate the power vector into a single constraint) does not perfectly fit the data. The power profiles for the minimum-energy transition show that the lift rotors do very little. In fact, they are only used initially to slightly arrest the descent in order to avoid violating the maximum acceleration constraint. The cruise rotor power shows that initially maximum power is used to reach a velocity at which the aircraft can rely on wing-based lift, followed by a gradual climb at reduced power.

Next, we present two more trajectories that demonstrate the versatility of the fast surrogate modeling approach (Figure 8). Both these trajectories have additional constraints that mimic possible operating constraints for proposed air-taxi missions. First, we find a minimum energy constant-altitude transition trajectory. This includes one added constraint that the minimum altitude cannot be less than the initial altitude. This trajectory is modeled after the proposed mission profiles by Silva [4], which contain a constant-altitude transition segment. Second, we model a complete takeoff (transition plus climb) trajectory. We add two additional constraints: the altitude cannot be less than zero to avoid ground collisions and the aircraft must reach cruise conditions by 3 km.

The constant-altitude transition trajectory in Figure 8 shows that the aircraft pitches down initially, followed by a rapid pitch-up maneuver all by 500 m. In this case, the initial nose-down maneuver corresponds with the lowest drag configuration which enables the most efficient acceleration. Once the velocity becomes large enough, the aircraft pitches upwards to utilize lift generated

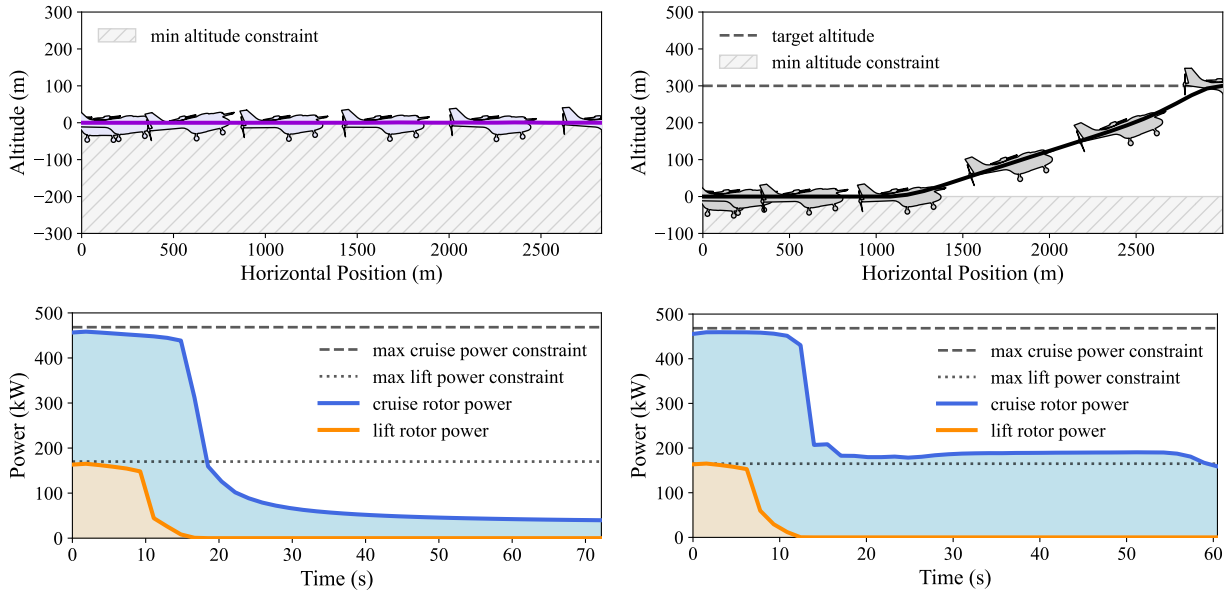

Figure 8: Left: the constant-altitude, minimum-energy transition trajectory. Right: the minimum-energy takeoff (transition plus climb) trajectory.

by the wing. As the velocity further increases, the pitch angle can gradually reduce such that the lift matches the weight. The minimum energy takeoff trajectory in Figure 8 includes a low-altitude acceleration followed by a gradual climb. Similar to the other trajectories shown here, this minimizes the use of the lifting rotors and maximizes the time spent in an airplane-mode of flight. However, this trajectory is perhaps impractical because it would require future air-taxi hubs to include a long, flat, and unpopulated corridor within which an air taxi could perform the early acceleration.

As before, we compare the time-histories of the lift and cruise rotor power (Figure 8) to gain insight on the trajectories. Both of these trajectories contain a nearly identical initial high-power acceleration. In fact, the only noticeable difference is that the cruise rotor power for the takeoff trajectory is higher during the latter half of the trajectory to sustain the climb to 300 m altitude. The cruise rotor power for the constant-altitude trajectory decreases gradually as the aircraft approaches the target cruise speed.

Table 3: Numerical results for the minimum-energy and minimum-time trajectories

	Energy (MJ / Wh)	Time (s)	Efficiency (%)
Minimum-energy transition	11.4 / 3167	67.2	47.4
Minimum-time transition	28.1 / 7806	15.7	19.2
Minimum-energy constant-altitude transition	27.0 / 7500	64.2	20.0
Minimum-time constant-altitude transition	37.9 / 10528	22.1	14.2
Minimum-energy takeoff	35.3 / 9806	62.0	27.8

The numerical data for the four trajectories presented in this section is summarized in Table 3. For comparison Table 3 also includes a minimum-time constant-altitude transition trajectory that is not shown in any figure because it is visually the same in profile as the minimum-energy constant-altitude transition in Figure 8.

3.2 Constrained Transition Trajectories

The optimal trajectories presented in Section 3.1 contain behaviors that are not necessarily desirable for real-world air-taxi operations (e.g., the minimum energy transition contains large altitude fluctuations and the constant-altitude transition requires more than 3 km of horizontal distance). In this section, we present results that show the sensitivity of the minimum-energy transition trajectories to constraints on horizontal distance and altitude.

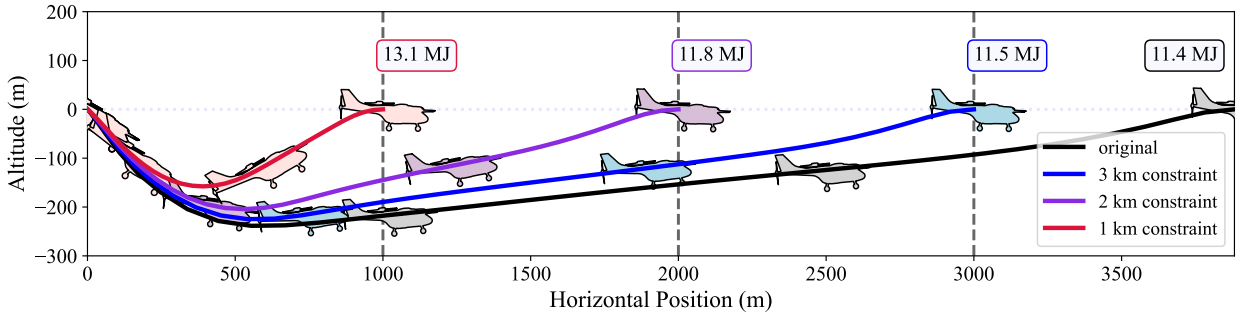

Figure 9: Minimum-energy transition trajectories with horizontal displacement constraints.

The trajectories in Figure 9 are variants of the minimum-energy transition trajectory in Figure 7 with one additional constraint on the maximum allowable horizontal position. These results show that the energy design space is relatively flat with respect to this constraint. Constraining the aircraft to transition within 1 km results in only 15% more energy consumption than the original, unconstrained transition trajectory.

Next, we show minimum energy transition trajectories with altitude-loss constraints in Figure 10. The original trajectory in Figure 7 is impractical because it requires a high initial altitude (e.g., takeoff from the top of a tall building). If this initial altitude is much lower, the optimal trajectories will have a minimum altitude constraint like we show in Figure 10. As the altitude constraint becomes more aggressive we find that the energy expenditure increases. Finally, as the constraint on altitude loss reaches 0 m, we recover the same constant-altitude transition trajectory from Figure 8. This trajectory requires 138% more energy than the unconstrained trajectory. Based on these results, it is evident that, if given the chance, minimum-energy transition trajectories will exploit a trade of potential for kinetic energy. A final observation is that the constant-altitude transition trajectory requires more horizontal distance to reach cruise than either of the trajectories with 50 m and 100 m altitude-loss constraints. This is unexpected because there appears to be a trend of decreasing horizontal distance with increasingly restrictive altitude-loss constraints. This behavior is somewhat explained because the aircraft cannot dive to gain velocity due to the constant-altitude constraint. Instead, it accelerates horizontally and travels farther than expected.

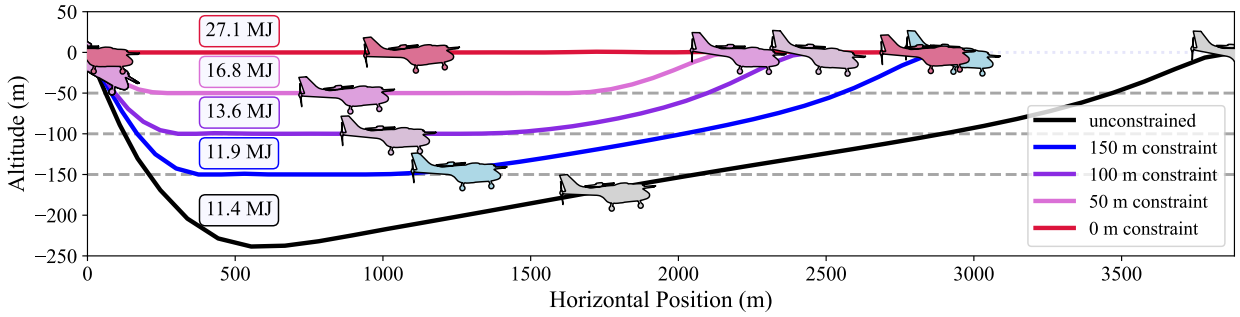

Figure 10: Minimum-energy transition trajectories with altitude-loss constraints.

3.3 Takeoff with a No-Fly Zone

The takeoff trajectory in Figure 8 contains low-altitude, high-speed flight that may pose regulatory and safety issues for commercial UAM missions. In this section we present a minimum-energy takeoff trajectory with a no-fly zone constraint. We formulate this constraint to force a near-vertical liftoff, followed by a transition and climb that must occur above 100 m. Because this trajectory contains three distinct segments (liftoff, transition, and climb), it represents a complete optimization of the pre-cruise portion of proposed UAM mission profiles [4, 5]. The results of this optimization are shown in Figure 11.

The minimum-energy takeoff trajectory in Figure 11 contains two additional constraints: the minimum altitude must be greater than the no-fly zone and the maximum horizontal displacement must be less than 3 km. Upon inspection, the trajectory in Figure 11 is a composite of the constant-altitude transition trajectory and the takeoff trajectory in Figure 8. The aircraft lifts off in hover, and climbs to 100 m (tightly following the no-fly zone profile) using the full power of both the lift rotors and the cruise rotor. This is followed by a constant-altitude transition at 100 m and a steady climb to 300 m. The addition of the no-fly zone requires 67% more energy than the unconstrained takeoff trajectory (Figure 8) and requires ten more seconds to complete. Because this trajectory is heavily constrained, the optimization problem requires nearly two hours to converge to a solution.

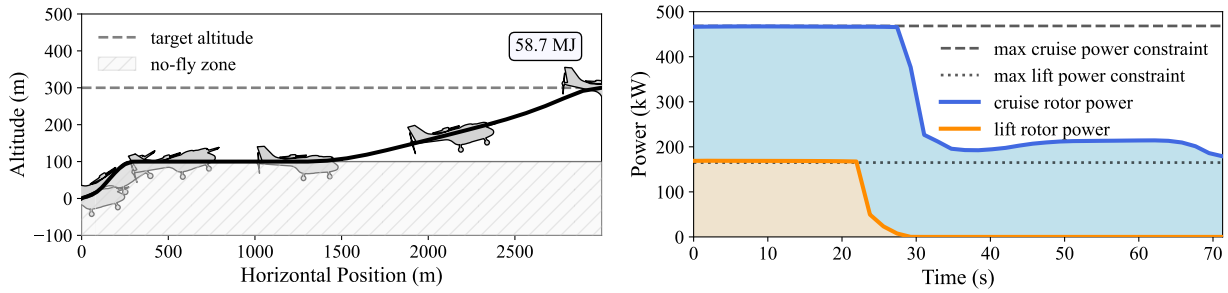

Figure 11: Left: the minimum-energy takeoff trajectory with a no-fly zone constraint. Right: the corresponding power time-histories for the minimum-energy takeoff trajectory (left).

4 Conclusion

In this paper, we presented the results of 12 variants of the takeoff and transition trajectory optimization problem for NASA's Lift-plus-Cruise air-taxi concept. These results demonstrate the versatility and robustness of the fast surrogate modelling approach. This approach allows us to simulate realistic air-taxi trajectories that are representative of real UAM missions. The contribution of this paper is as follows: (a) we introduce a novel, surrogate-based aircraft trajectory optimization framework, and (b) we present optimal air-taxi transition and takeoff trajectories.

This study provides insight into the solution-space for the air-taxi trajectory design problem. For example, we find that the Lift-plus-Cruise air taxi can transition from hover to cruise in as little as 16 seconds; however, this requires nearly 200% more energy than trajectories which complete the transition in roughly 60 seconds. Many proposed air-taxi mission profiles include a near-vertical liftoff followed by a transition to cruise at a substantial altitude. This makes sense when considering these aircraft must operate in or near urban areas. However, the takeoff trajectories presented here shows that low-altitude transition uses 40% less energy than the trajectories that include a vertical liftoff and a higher-altitude transition. These examples are indicative of the trade-offs that air-taxi designers face when considering commercial UAM operations.

We recognize certain limitations and/or assumptions in this work. The models used are of low fidelity. Specifically, the aerodynamic model is incapable of modeling any rotor-wing interactions, and the rotor model cannot model negative axial inflow velocities. This means, among other things, that these models can only be applied to forward transitions and takeoff trajectories because the reverse (cruise to hover) transition could include regimes where the rotors fly into their own wake.

Direct methods for solving trajectory optimization problems are notorious for requiring good initial guesses for the control inputs. Without these, the solution diverges or converges to sub-optimal local minima. The methods presented here are also susceptible to these potential pitfalls. However, the robustness of the surrogate models signifies that the optimizer can recover from poor initial trajectories without encountering any numerical difficulties.

Acknowledgments

The material presented in this paper is, in part, based upon work supported by NASA under award No. 80NSSC21M0070 and by DARPA under grant No. D23AP00028-00.

References

[1] Darshan Sarojini, Marius L Ruh, Anugrah Jo Joshy, Jiayao Yan, Alexander K Ivanov, Luca Scotzniovsky, Andrew H Fletcher, Nicholas C Orndorff, Mark Sperry, Victor E Gandarillas, et al. "Large-Scale Multidisciplinary Design Optimization of an eVTOL Aircraft using Comprehensive Analysis". In: *AIAA SCITECH 2023 Forum*. 2023, p. 0146. DOI: 10.2514/6.2023-0146.

[2] Marius Ruh, Anugrah Jo Joshy, Andrew Fletcher, Isaac Asher, and John Hwang. "Large-scale multidisciplinary design optimization of the NASA lift-plus-cruise concept using a novel aircraft design framework". In: *VFS*. 2023. DOI: 10.48550/arXiv.2304.14889.

[3] John T Hwang and Andrew Ning. "Large-scale multidisciplinary optimization of an electric aircraft for on-demand mobility". In: *2018 AIAA/ASCE/AHS/ASC Structures, Structural Dynamics, and Materials Conference*. 2018. DOI: 10.2514/6.2018-1384.

[4] Christopher Silva, Wayne R Johnson, Eduardo Solis, Michael D Patterson, and Kevin R Antcliff. "VTOL urban air mobility concept vehicles for technology development". In: *2018 Aviation Technology, Integration, and Operations Conference*. 2018, p. 3847. DOI: 10.2514/6.2018-3847.

[5] Michael D Patterson, Kevin R Antcliff, and Lee W Kohlman. "A proposed approach to studying urban air mobility missions including an initial exploration of mission requirements". In: *Annual Forum and Technology Display*. NF1676L-28586. 2018.

[6] Shamsheer S Chauhan and Joaquim RRA Martins. "Tilt-wing eVTOL takeoff trajectory optimization". In: *Journal of aircraft* 57.1 (2020), pp. 93–112. DOI: 10.2514/1.C035476.

[7] Ryan Anderson, Jacob Willis, Jake Johnson, Andrew Ning, and Randal W Beard. "A comparison of aerodynamics models for optimizing the takeoff and transition of a bi-wing tailsitter". In: *AIAA Scitech 2021 Forum*. 2021, p. 1008. DOI: 10.2514/6.2021-1008.

[8] John T Betts. "Survey of numerical methods for trajectory optimization". In: *Journal of guidance, control, and dynamics* 21.2 (1998), pp. 193–207. DOI: 10.2514/2.4231.

[9] Shugo Kaneko and Joaquim RRA Martins. "Simultaneous Optimization of Conceptual Design and Takeoff Trajectory of a Lift-Plus-Cruise UAV". In: *10th Autonomous VTOL Technical Meeting* (2023).

[10] Matthew P. Kelly. "An introduction to trajectory optimization: How to do your own direct collocation". In: *SIAM Review* 59.4 (2017), pp. 849–904. DOI: 10.1137/16M1062569.

[11] Matthew P Kelly. "Transcription methods for trajectory optimization: a beginners tutorial". In: *arXiv* (2017). DOI: 10.48550/arXiv.1707.00284.

[12] Richard S Sutton and Andrew G Barto. *Reinforcement learning: An introduction*. MIT press, 2018, pp. 73–90.

[13] Oskar Von Stryk and Roland Bulirsch. "Direct and indirect methods for trajectory optimization". In: *Annals of operations research* 37 (1992), pp. 357–373. DOI: 10.1007/BF02071065.

[14] Charles R Hargraves and Stephen W Paris. "Direct trajectory optimization using nonlinear programming and collocation". In: *Journal of guidance, control, and dynamics* 10.4 (1987), pp. 338–342. DOI: 10.2514/3.20223.

[15] Arthur Earl Bryson and Walter F Denham. "A steepest-ascent method for solving optimum programming problems". In: *Journal of Applied Mechanics* (1962). DOI: 10.1115/1.3640537.

[16] John T Hwang and Drayton Munster. "Solution of ordinary differential equations in gradient-based multidisciplinary design optimization". In: *2018 AIAA/ASCE/AHS/ASC Structures, Structural Dynamics, and Materials Conference*. 2018. DOI: 10.2514/6.2018-1646.

[17] Joaquim R R A Martins and John T Hwang. "Review and unification of methods for computing derivatives of multidisciplinary computational models". In: *AIAA journal* 51.11 (2013), pp. 2582–2599. DOI: 10.2514/1.J052184.

[18] John T. Hwang and Joaquim R. R. A. Martins. "A Computational Architecture for Coupling Heterogeneous Numerical Models and Computing Coupled Derivatives". In: *ACM Trans. Math. Softw.* 44.4 (June 2018), 37:1–37:39. ISSN: 0098-3500. DOI: 10.1145/3182393.

[19] Lars Blackmore, Behçet Açikmeşe, and Daniel P Scharf. "Minimum-landing-error powered-descent guidance for Mars landing using convex optimization". In: *Journal of guidance, control, and dynamics* 33.4 (2010), pp. 1161–1171. DOI: 10.2514/1.47202.

[20] John T Betts and Evin J Cramer. "Application of direct transcription to commercial aircraft trajectory optimization". In: *Journal of Guidance, Control, and Dynamics* 18.1 (1995), pp. 151–159. DOI: 10.2514/3.56670.

[21] John T Betts. *Practical methods for optimal control and estimation using nonlinear programming*. SIAM, 2010.

[22] Charles Hargraves, Forrester Johnson, Stephen Paris, and Ian Retties. "Numerical computation of optimal atmospheric trajectories". In: *Journal of Guidance and Control* 4.4 (1981), pp. 406–414. DOI: 10.2514/3.56093.

[23] Robert D Falck, Jeffrey Chin, Sydney L Schnulo, Jonathan M Burt, and Justin S Gray. "Trajectory optimization of electric aircraft subject to subsystem thermal constraints". In: *18th AIAA/ISSMO Multidisciplinary Analysis and Optimization Conference*. 2017, p. 4002. DOI: 10.2514/6.2017-4002.

[24] Pramudita Satria Palar, Rhea Patricia Liem, Lavi Rizki Zuhal, and Koji Shimoyama. "On the use of surrogate models in engineering design optimization and exploration: The key issues". In: *Proceedings of the Genetic and Evolutionary Computation Conference Companion*. 2019, pp. 1592–1602. DOI: 10.1145/3319619.3326813.

[25] Xiaosong Du, Ping He, and Joaquim RRA Martins. "Rapid airfoil design optimization via neural networks-based parameterization and surrogate modeling". In: *Aerospace Science and Technology* 113 (2021), p. 106701. DOI: 10.1016/j.ast.2021.106701.

[26] Yolanda Mack, Tushar Goel, Wei Shyy, and Raphael Haftka. "Surrogate model-based optimization framework: a case study in aerospace design". In: *Evolutionary computation in dynamic and uncertain environments* (2007), pp. 323–342. DOI: 10.1007/978-3-540-49774-5_14.

[27] Daniel L Clark Jr, Darcy L Allison, Harok Bae, and Edwin E Forster. "Effectiveness-based design of an aircraft considering mission uncertainties". In: *Journal of Aircraft* 56.5 (2019), pp. 1961–1972. DOI: 10.2514/1.C035402.

[28] Mohamed Amine Bouhlel, John T. Hwang, Nathalie Bartoli, Rémi Lafage, Joseph Morlier, and Joaquim R. R. A. Martins. "A Python surrogate modeling framework with derivatives". In: *Advances in Engineering Software* (2019), p. 102662. ISSN: 0965-9978. DOI: https://doi.org/10.1016/j.advengsoft.2019.03.005.

[29] Paul Saves, Remi Lafage, Nathalie Bartoli, Youssef Diouane, Jasper Bussemaker, Thierry Lefebvre, John T Hwang, Joseph Morlier, and Joaquim RRA Martins. "SMT 2.0: A Surrogate Modeling Toolbox with a focus on Hierarchical and Mixed Variables Gaussian Processes". In: *arXiv* (2023). DOI: 10.48550/arXiv.2305.13998.

[30] Wayne Johnson, Christopher Silva, and Eduardo Solis. "Concept vehicles for VTOL air taxi operations". In: *AHS Specialists"Conference on Aeromechanics Design for Transformative Vertical Flight*. ARC-E-DAA-TN50731. 2018.

[31] Victor Gandarillas, Anugrah Jo Joshy, Mark Z. Sperry, Alexander Ivanov, and John T Hwang. "A graph-based methodology for constructing computational models that automates adjoint-based sensitivity analysis". In: *Structural and Multidisciplinary Optimization* (2023).

[32] Nicholas C Orndorff and John T Hwang. "Investigation of Optimal Air-Taxi Transition Profiles using Direct-Transcription Trajectory Optimization". In: *AIAA AVIATION 2022 Forum*. 2022, p. 3485. DOI: 10.2514/6.2022-3485.

[33] Dale Marvin Pitt. *Rotor dynamic inflow derivatives and time constants from various inflow models*. Washington University in St. Louis, 1980.

[34] Dale M Pitt. "Theoretical prediction of dynamic inflow derivatives". In: *Vertica* 5 (1981), pp. 21–34.

[35] John T Hwang and Joaquim R R A Martins. "A fast-prediction surrogate model for large datasets". In: *Aerospace Science and Technology* 75 (2018), pp. 74–87. DOI: 10.1016/j.ast.2017.12.030.

[36] Martin Dietrich Buhmann. "Radial basis functions". In: *Acta numerica* 9 (2000), pp. 1–38. DOI: 10.1080/00107510903372134.

[37] Robert A. McDonald and James R. Gloudemans. "Open Vehicle Sketch Pad: An Open Source Parametric Geometry and Analysis Tool for Conceptual Aircraft Design". In: *AIAA SCITECH 2022 Forum* (2022). DOI: 10.2514/6.2022-0004.

[38] Justin L Petrilli, Ryan C Paul, Ashok Gopalarathnam, and Neal T Frink. "A CFD database for airfoils and wings at post-stall angles of attack". In: *31st AIAA applied aerodynamics conference*. 2013, p. 2916. DOI: 10.2514/6.2013-2916.

[39] Robert E Sheldahl and Paul C Klimas. *Aerodynamic characteristics of seven symmetrical airfoil sections through 180-degree angle of attack for use in aerodynamic analysis of vertical axis wind turbines*. Tech. rep. Sandia National Labs., Albuquerque, NM (USA), 1981. DOI: 10.2172/6548367.

[40] Nan Hnin Hnin Htwe. "Design of 50 kw Permanent Magnet Synchronous Motor for HEV". In: *IRE* 3 (2019).

[41] Dongyun Lu and Narayan C Kar. "A review of flux-weakening control in permanent magnet synchronous machines". In: *2010 IEEE Vehicle Power and Propulsion Conference*. IEEE. 2010, pp. 1–6. DOI: 10.1109/VPPC.2010.5728986.

[42] SF Zhao, XY Huang, YT Fang, and J Li. "A control scheme for a High Speed Railway traction system based on high power PMSM". In: *2015 6th International Conference on Power Electronics Systems and Applications (PESA)*. IEEE. 2015, pp. 1–8. DOI: 10.1109/PESA.2015.7398905.

[43] I Wakefield and C Dubuque. "Exceeding tire speed rating during takeoff". In: *Boeing AERO Quarterly* (2009).

[44] JW Gebhard. "Acceleration and comfort in public ground transportation". In: *The National Academies of Sciences, Engineering, and Medicine* (1970).

[45] G Kreisselmeier and R Steinhauser. "Systematic control design by optimizing a vector performance index". In: *Computer aided design of control systems*. Elsevier, 1980, pp. 113–117. DOI: 10.1016/S1474-6670(17)65584-8.

[46] Philip E Gill, Walter Murray, and Michael A Saunders. "SNOPT: An SQP algorithm for large-scale constrained optimization". In: *SIAM review* 47.1 (2005), pp. 99–131. DOI: 10.1137/S0036144504446096.